On mechanisms for HF pump-enhanced optical emissions at 557.7 and 630.0 nm from atomic oxygen in the high-latitude F-region ionosphere

Thomas B. Leyser[1], Tima Sergienko[2], Urban Brändström[2], Björn Gustavsson[3], and Michael T. Rietveld[4]

[1]Swedish Institute of Space Physics, Uppsala, Sweden.
[2]Swedish Institute of Space Physics, Kiruna, Sweden.
[3]Department of Physics and Technology, The Arctic University of Norway, Tromsø, Norway.
[4]Scientist emeritus, EISCAT Scientific Association, Ramfjordmoen, Norway.

Correspondence: Thomas Leyser (thomas.leyser@irfu.se)

Abstract. The EISCAT Heating facility was used to transmit powerful high frequency (HF) electromagnetic waves into the F-region ionosphere to enhance optical emissions at 557.7 and 630.0 nm from atomic oxygen. The emissions were imaged by three stations of the Auroral Large Imaging System in northern Sweden and the EISCAT UHF incoherent scatter radar was used to obtain plasma parameter values. The ratio of the 557.7 to 630.0 nm column emission rates changed from $I_{5577}/I_{6300} \approx 0.2$

5   for the HF pump frequency $f_0 = 6.200$ MHz $\approx 4.6 f_\mathrm{e}$ to $I_{5577}/I_{6300} \approx 0.5$ when $f_0 = 5.423$ MHz $\lesssim 4 f_\mathrm{e}$, where f_e is the ionospheric electron gyro frequency. The observations are interpreted in terms of decreased electron heating efficiency and thereby weaker enhancement at 630.0 nm for $f_0 = 5.423$ MHz $\lesssim 4 f_\mathrm{e}$. The emissions at 557.7 nm are attributed to electron acceleration by upper hybrid waves of meter-scale wavelengths that can be excited with $f_0 = 5.423$ MHz $\lesssim 4 f_\mathrm{e}$.

1 Introduction

10   Powerful high frequency (HF) electromagnetic waves transmitted into the ionosphere from the ground may enhance optical emissions from atmospheric constituents, notably atomic oxygen and molecular nitrogen. Such emissions can be detected on the ground and are studied to get information on a variety of phenomena related to plasma energization by HF pumping. Following the first unambiguous observations of HF pump-enhanced optical emissions at high latitudes (Brändström et al., 1999; Kosch et al., 2002b), a number of interesting results have been obtained. Here we limit ourselves to HF pumping with

15   the frequency f_0 below or near the ionospheric critical frequency and with left-handed circular polarization (often referred to as ordinary mode) which gives the strongest effects.

     The spatial distribution of optical emissions enhanced above background levels has shown that the strongest coupling between an HF beam and the ionospheric F-region plasma at high latitudes and long time scales occurs for a beam in the direction of geomagnetic zenith. Even with a vertical beam, the most intense optical emissions occur towards magnetic zenith within the

20   beam. This was observed in emissions at 630.0 nm from the O(^{1}D) excited state as obtained with the EISCAT (European Incoherent Scatter association) Heating facility in Norway (Kosch et al., 2000), with the Sura facility in Russia (Grach et al., 2007; Shindin et al., 2015), as well as with the HAARP (High Frequency Active Auroral Research Program) facility in Alaska, USA

(Pedersen and Carlson, 2001), and also at 557.7 nm from O(^{1}S) (Pedersen et al., 2003, 2008). In addition, optical emissions show evidence of complex HF beam re-organization during pumping and associated nonlinear effects in the pump–plasma interactions, as found in experiments both at EISCAT and HAARP (Kosch et al., 2004, 2007).

Imaging of enhanced optical emissions from several stations with the Auroral Large Imaging System (ALIS) in northern Sweden and HF transmissions with EISCAT Heating provided for the first tomography-like reconstruction of the volume emission at 630.0 nm (Gustavsson et al., 2001). By comparing the obtained altitude and temporal variations of the optical emissions with modelled emissions of excitation of O(^{1}D) by a maxwellian electron velocity distribution, the authors predicted the source distribution for the emissions to be maxwellian at low energies but with a depletion above 1.96 eV (which is the threshold for the excited state).

Observation of optical emissions simultaneously at several wavelengths, each requiring different minimum electron energy to be enhanced, provides the possibility to study electron energization in the excited plasma turbulence. Gustavsson et al. (2002) obtained nearly simultaneous images of enhancements at 557.7 and 630.0 nm in experiments with EISCAT Heating. The 557.7 to 630.0 nm intensity ratio of 0.3–0.4 was relatively high which implies that the optical enhancements were caused by a nonthermal tail in the electron velocity distribution. A similarly high ratio has been observed in experiments with HAARP (Pedersen et al., 2003).

Gustavsson and Eliasson (2008) observed emissions at 427.8, 557.7, 630.0 and 844.6 nm, together with incoherent scatter radar measurements of the ion temperature, electron temperature and concentration at EISCAT. By using a two-stream electron transport code they could estimate the electron flux between 1.9 and 100 eV that is needed to account for the observations. The electron energy distribution was found to be depleted approximately in the range 2–4 eV, probably due to excitation of vibrational states in N_2, and have a nonthermal tail at higher energies.

Experimental results on pump-enhanced optical emissions have been presented for varying f_0 near an harmonic s ($s = 3$, 4) of the ionospheric electron gyro frequency f_e. Kosch et al. (2002a) observed simultaneously emissions at 630.0 nm and small-scale geomagnetic field-aligned density striations with the CUTLASS coherent scatter radar. They found a significant reduction in the optical enhancement and the radar backscatter when $f_0 \approx 3f_e$, indicating that the 630.0 nm emissions are linked to upper hybrid turbulence and filamentary striations.

Further, Gustavsson et al. (2006) performed EISCAT experiments with f_0 stepping near sf_e ($s = 3$, 4) and optical imaging at 630.0, 557.7 and 427.8 nm together with incoherent scatter radar measurements of the electron temperature. The pump-enhanced emissions as well as electron temperature were all minimum for $f_0 \approx 4f_e$. Whereas the enhancement of the emission intensity at 630.0 nm and electron temperature were roughly symmetric for f_0 around $4f_e$, the emissions at 427.8 nm were markedly stronger for f_0 of few tens of kilohertz above sf_e. This suggests that there are different electron energization processes underlying the emissions at 630.0 nm and 427.8 nm. The observations at 427.8 nm were the first direct evidence of pump-induced ionization of thermospheric N_2. The experimental results are consistent with theory that predict electron acceleration by upper hybrid oscillations localized in cylindrical density depletions and formation of a suprathermal tail in the electron velocity distribution (Istomin and Leyser, 2003; Najmi et al., 2017). The acceleration efficiency is the largest for f_0 slightly above sf_e for $s \geq 3$.

To further analyze these experimental results, Sergienko et al. (2012) performed Monte Carlo simulations of the transport of energized electrons into the ambient thermosphere. The observed 630.0 nm emissions could be accounted for by predominantly thermal electrons (> 70 % of the emission intensity), with accelerated electrons playing a minor role for the emissions. However, to explain the emission intensity at 427.8 nm, electrons must be accelerated to 60 eV or more.

Shindin et al. (2015) observed emissions at 557.7 and 630.0 nm at the Sura facility for f_0 near $4f_e$, an ERP of about 100 MW and the HF beam directed either vertically or tilted $12°$ south from the vertical in the magnetic meridional plane towards magnetic zenith ($19°$ south). Simultaneous observations of the frequency spectrum of stimulated electromagnetic emissions were used to determine where f_0 was relative to $4f_e$. The pump-enhanced 630.0 nm emissions did not exhibit a dependence on f_0 near $4f_e$. And no minimum in the optical emission intensities was observed when $f_0 \approx 4f_e$, which is contrary to previous measurements by others as mentioned above. The authors attribute this to natural variations in the ionospheric interaction altitudes during the experiments. Further, the authors found that for a vertical HF beam, 557.7 nm emissions occurred for f_0 about 5–15 kHz below $4f_e$ and also at about 220–280 kHz above $4f_e$. With the HF beam directed towards magnetic zenith, pump-enhanced emissions were observed for f_0 about 15–20 kHz above $4f_e$.

In addition to these results for $f_0 \gtrsim 3f_e$, a number of interesting experiments and theories have been presented for f_0 near $2f_e$, but those are outside the scope of the present paper, as the relevant dispersion properties of electron Bernstein and upper hybrid modes are different for $s = 2$ and $s \geq 3$. Here we are concerned with f_0 near $4f_e$ and higher.

2 Experiment setup

The EISCAT Heating facility (Rietveld et al., 2016) was used to transmit HF waves in the cycle of 150 s on/85 s off with the beam pointing in geomagnetic zenith ($\sim 78°$ elevation south) and with left-handed circularly polarization (ordinary mode), on 16 February 2015. From 16:00:00 to 16:49:30 UT, $f_0 = 6.200$ MHz and the effective radiative power (ERP) was approximately 138 MW. To keep f_0 below the decreasing ionospheric ordinary-mode critical frequency after sunset, $f_0 = 5.423$ MHz from 16:50:55 to 17:09:05 UT and the ERP was 116 MW. Local time was UT+1 hour.

Optical emissions were observed with the ALIS stations in Abisko, Kiruna and Tjautjas. The cameras had a field of view of $60°$ and gave an image size of 512×512 pixels with a temporal resolution of 7 s. Emissions were imaged at 427.8 nm from N_2^+(1NG) with a threshold of 18.6 eV (Holma et al., 2006), 557.7 nm from O(^{1}S) with the threshold 4.17 eV (Haslett and Megill, 1974), 630.0 nm from O(^{1}D) with the threshold 1.96 eV (Haslett and Megill, 1974), and 844.6 nm from O($3p^3$P) with the threshold 10.99 eV (Gustavsson et al., 2005). Kvammen et al. (2019) analyzed all four emission lines for this same experiment and presented tomography-like reconstructions of the three-dimensional distribution of the optical volume emission rates. However, in the present treatment we focus on the 557.7 and 630.0 nm lines which are the strongest and for which we have the most data. As the emissions were imaged from three sites, we too employed tomography-like inversion to get the volume emission rates for the two spectral lines, along the lines described by Gustavsson et al. (2001).

The EISCAT UHF incoherent scatter radar was operated with a meridional scan pattern to measure background plasma parameter values at different angles to the geomagnetic field, using the beata program with a temporal resolution of 5 s and
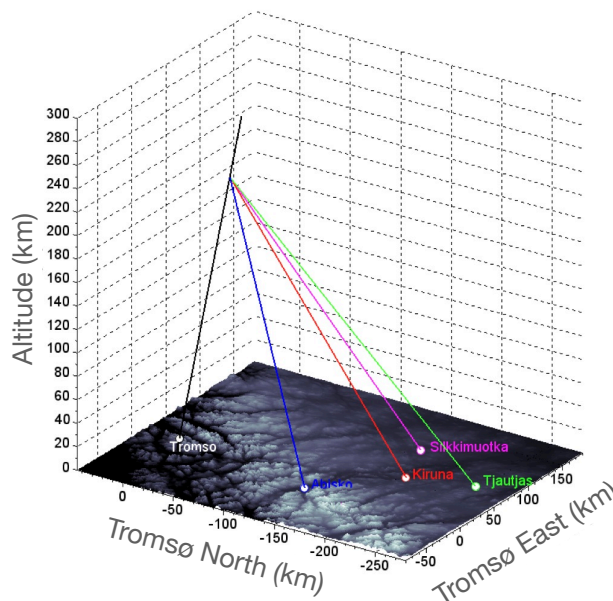
Figure 1. Illustration of the relative positions of the EISCAT facilities at the Ramfjordmoen site outside Tromsø, Norway, and the ALIS stations in the Kiruna region, Sweden. The black line shows the direction of magnetic zenith. The ALIS station at Silkkimuotka was not used in the experiments.

altitude resolution of approximately 3 km. Figure 1 shows the geometry of the experiment with the relative positions of the EISCAT facilities at the Ramfjordmoen site outside Tromsø, Norway, and the ALIS stations in the Kiruna region, Sweden.

Stimulated electromagnetic emission were received on the ground in Kroken (Tromsø), but were weak and only rarely exhibited spectral structure. Ionograms from the EISCAT Dynasonde show elevated D-region absorption.

95 3 Experimental results

Figure 2 shows an overview of the time development of the altitude profile of the pump-enhanced optical emissions at 630.0 nm above background as observed from the three ALIS sites. The column emission rate weakened as f_0 was changed from 6.200 MHz to 5.423 MHz at about 16:50 UT. For the second HF pulse at $f_0 = 5.423$ MHz observed at the Abisko station, the relatively short duration shown in the enhancement is due to lacking synchronization between the pump wave and optical
100 filter wheel sequence. The slow growth of the emission intensity and extension towards higher altitudes during the pump pulses can be seen. Also, the emissions occurred at lower altitudes for the lower f_0. Figure 3 displays similarly an overview of the emissions at 557.7 nm for the same time period. The emission intensity did not weaken as f_0 was decreased at about 16:50 UT. The images from the Kiruna site show even an increase in the emissions as f_0 was decreased, despite a lower ERP. But again the altitude region of the emissions decreased as f_0 was lowered. It is interesting that Kvammen et al. (2019) observed a
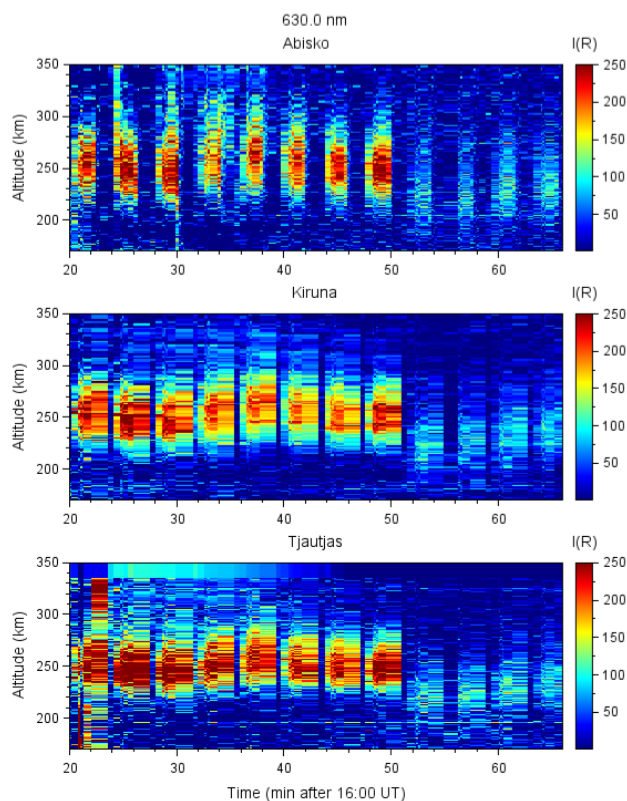
Figure 2. Overview of the column emissions at 630.0 nm from 16:00:00 to 17:09:05 UT on 16 February 2015. From 16:00:00 to 16:49:30 UT, $f_0 = 6.200$ MHz, and from 16:50:55 to 17:09:05 UT, $f_0 = 5.423$ MHz.

clear intensity increase in the 844.6 nm line which has a threshold of 10.99 eV, which similarly to the threshold of 4.17 eV of the 557.7 nm line is several times above the threshold of 1.96 eV for 630.0 nm.

Figure 4 shows the altitude profiles of the electron density, electron temperature and ion temperature obtained with the EISCAT UHF radar in geomagnetic zenith. Clear pump-induced enhancements in the electron temperature can be seen which are slowly conducted upward in the ionosphere with time, along the geomagnetic field where the thermal conductivity is the highest. The electron density and ion temperature did not exhibit notable pump-induced modulations. However, the electron density slowly decreased with time as the experiments occurred shortly after sunset.

Figure 5 shows the altitude profiles of the volume emission rates at 630.0 nm (left) and 557.7 nm (right) for the last pump cycle at $f_0 = 6.200$ MHz, as obtained by tomography-like reconstruction of the emission regions. The maximum volume emission rates occurred at approximately the same height for the two spectral lines, near $h_{\max} \approx 239$ km. The altitude profile for the 557.7 nm emission is wider than that for 630.0 nm, which. is consistent with that the excitation threshold for the former (4.17 eV) is higher, and the electrons having a longer mean free path, compared to the latter (1.96 eV). The times for the plotted profiles are determined by the sequence in the filter wheels for the ALIS cameras. Figure 6 shows similarly the height profiles
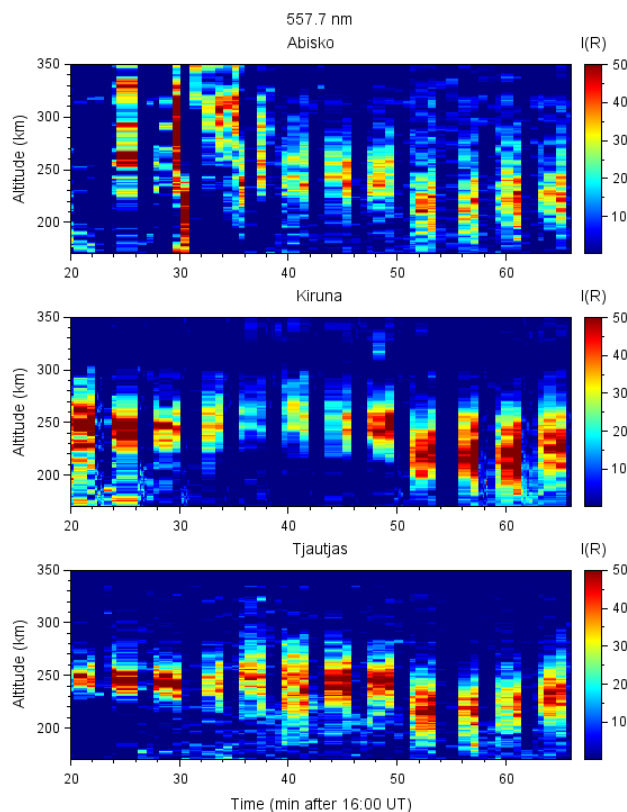
Figure 3. Similar to Fig. 2, but for the emissions at 557.7 nm.

of the volume emission rate for the third pump pulse at $f_0 = 5.423$ MHz. In this case, the maximum of the emissions at 557.7 nm (right) occurred about 7–10 km below that at 630.0 nm (left). Also, by comparing Figs. 5 and 6, we see that the emission rates for both lines grow slower with $f_0 = 5.423$ MHz.

Figure 7 summarizes the temporal evolution of the column emission rates at 630.0 nm (left) and 557.7 nm (right) during the growth phase following pump-on for $f_0 = 6.200$ MHz (red) and $f_0 = 5.423$ MHz (blue), for the same data as in Figs. 5 and 6. The 630.0 nm emissions are seen to be weaker for $f_0 = 5.423$ MHz than for $f_0 = 6.200$ MHz. However, the emission intensity at 557.7 nm is approximately the same for the two f_0 towards the end of the pump pulses. The intensity ratio towards the end of the plotted time interval is $I_{5577}/I_{6300} \approx 0.2$ for $f_0 = 6.200$ MHz and we observe $I_{5577}/I_{6300} \approx 0.5$ for $f_0 = 5.423$ MHz, which agrees with Kvammen et al. (2019) for the same experiment. We do not have data for the remaining part of the pump pulse of 150 s because of the used sequence for the filter wheels.
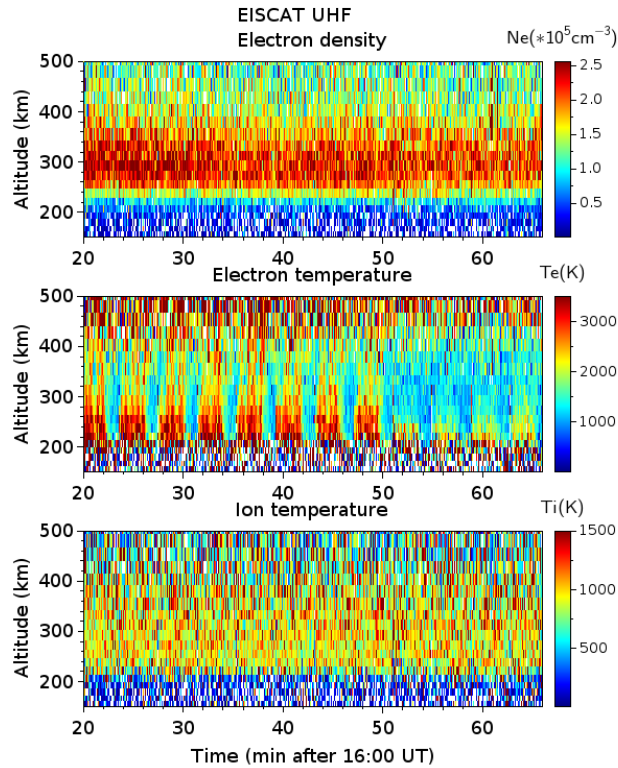
Figure 4. Overview of the electron density (top), electron temperature (center) and ion temperature (bottom) as obtained with the EISCAT UHF radar directed in magnetic zenith, from 16:00:00 to 17:09:05 UT on 16 February 2015. From 16:00:00 to 16:49:30 UT, $f_0 = 6.200$ MHz and from 16:50:55 to 17:09:05 UT, $f_0 = 5.423$ MHz.

4 Emission growth times

To obtain a measure of the growth time of the optical emissions after pump-on, we fit a theoretical growth time to the experimental data for the emission from a given excited state. The temporal evolution of an emission can be described by the continuity equation for the number density n_α of atoms in the excited state α (O(^{1}D), O(^{1}S)). n_α is related to the observed column emission rate I_λ through $n_\alpha(t) = I_\lambda(t)/A_\alpha/D_\lambda(t)$, where A_α is the Einstein coefficient(s) for the emission and D_λ is the observed spatial scale of the imaged optical region at the wavelength λ. The number density n_α is described by the equation

$$\frac{dn_\alpha}{dt} + \nabla \cdot (n_\alpha \mathbf{v}) = Q_\alpha(\mathbf{r},t) - L_\alpha(t)n_\alpha \tag{1}$$
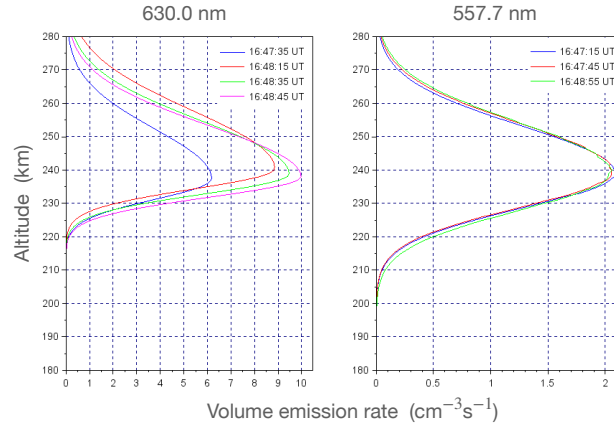
Figure 5. Temporal evolution of the height profile of the volume emission rates in magnetic zenith at 630.0 nm (left) and 557.7 nm (right) for $f_0 = 6.200$ MHz. The accuracy of the height determination is approximately ± 1 km.
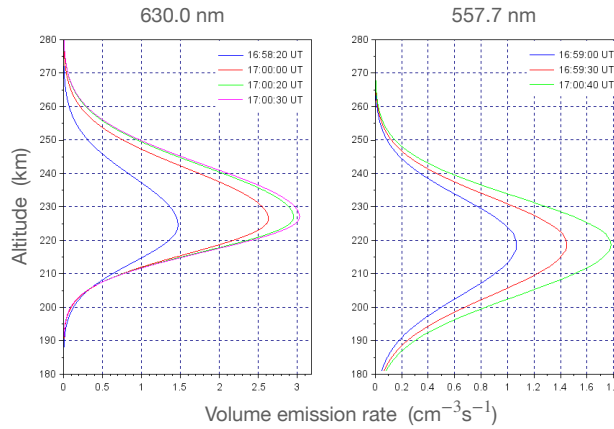
Figure 6. The same as Fig. 5, but for $f_0 = 5.423$ MHz.

where $Q_\alpha(t)$ is the excitation rate which includes the electron impact excitation (thermal and accelerated) and chemical reactions. The loss rate $L_\alpha(t)$ is given by

$$L_\alpha(t) = \sum_i (q_i n_i) - \sum_j A_j \tag{2}$$

where q_i is the rate coefficient for collisional de-excitation (quenching) by collisions with other species with the number density

140 n_i. The last term is the sum of the Einstein coefficients for all emissions originating from the excited state in question. For the 630.0 nm emission, $L_{\mathrm{O}(^1\mathrm{D})}$ includes the sum of three Einstein coefficients and q_i is for reactions with the main neutrals in the thermosphere at the heights of the F-region ionosphere (N_2, O_2 and O) as well as with thermal electrons. For the 557.7 nm line, $L_{\mathrm{O}(^1\mathrm{S})}$ is the sum of the Einstein coefficients only since the O(^{1}S) state is not quenched by collisions at the F-region
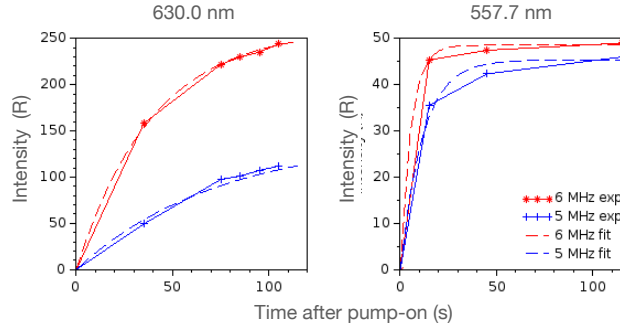
Figure 7. Temporal evolution of pump-enhanced column emission rates at 630.0 nm (left) and 557.7 nm (right) after pump-on at time $t = 0$ s, for the same pump pulses as in Figs. 5 and 6. The solid lines connect the data points shown by markers (red $*$ for $f_0 = 6.200$ MHz and blue $+$ for $f_0 = 5.423$ MHz). The dashed lines are the fits with Eq. (3) to obtain τ_{obs}.

Table 1. Emission growth times τ_{obs} after pump-on obtained by fitting Eq. (3) with the observed column emission rates at 630.0 nm (I_{6300}) and 557.7 nm (I_{5577}).

I_λ	f_0 (MHz)	τ_α (s)	τ_{obs} (s)
I_{6300}	6.200	40	39
I_{5577}	6.200	1.3	5.4
I_{6300}	5.423	25	74
I_{5577}	5.423	1.3	11

altitudes of the experiments. Further, for the experiment conditions, the term $\nabla \cdot (\mathbf{v} N)$ in Eq. (1) can be neglected because of

145   the low velocity $\mathbf{v}$ of the neutrals. For the purpose of the present analysis, the spatial dependencies of Q_α and L_α are neglected as we are interested only in a relatively small spatial region around the emission maximum, not in the entire emitting volume.

For our case of HF pump-enhanced emissions, the loss is constant with $L_\alpha = 1/\tau_\alpha$, where τ_α is the effective lifetime of the excited state α. For the O(^{1}S) state, $\tau_{\mathrm{O}(^1\mathrm{S})}$ equals the radiative lifetime so that $\tau_{\mathrm{O}(^1\mathrm{S})} = 1.3$ s, because this state is not quenched by collisions. For the O(^{1}D) state, $\tau_{\mathrm{O}(^1\mathrm{D})}$ is affected by quenching and we take $\tau_{\mathrm{O}(^1\mathrm{D})}$ for the relevant altitudes from

150   Gustavsson et al. (2001).

For the purpose of our analysis, we take the source term Q_α to be constant. The solution to Eq. (1) is

$$n_\alpha(t) = \tau Q_\alpha \left[1 - \exp\left(-\frac{t}{\tau} \right) \right] \tag{3}$$

With Q_α constant, the growth time is $\tau = \tau_\alpha$. However, for the general case when Q_α is time dependent, τ is determined by both the lifetime τ_α and $Q_\alpha(t)$. Therefore, if fitting the experimental data by Eq. (3) for which Q_α is constant, gives an

155   observed growth time τ_{obs} very different from τ_α, this implies that the source Q_α is not constant.

To obtain τ_{obs} from the measurements, we recall that $n_\alpha(t) = I_\lambda(t)/A_\alpha/D_\lambda(t)$, so that the observed intensity $I_\lambda(t) \propto n_\alpha(t)$ for a fixed D_λ. Thus, $I_\lambda(t)$ is fitted with a quantity proportional to Eq. (3) for the images at the different $t = t_i$ of the data. $I_\lambda(t_i)$ is averaged over a small square (15×15 pixels) around the maximum intensity in the images. The fitting is done by the least-squares Levenberg–Marquardt algorithm.

160   Table 1 summarizes τ_{obs} for the column emission rates at 557.7 and 630.0 nm. The theoretical lifetime $\tau_{\mathrm{O(^1D)}} \approx 40$ s in the third column from the left, is for the altitude $h_{\mathrm{max}} \approx 239$ km (Gustavsson et al., 2001) where the 630.0 nm volume emission rate is maximum for $f_0 = 6.200$ MHz (Fig. 5). Similarly, $\tau_{\mathrm{O(^1D)}} \approx 25$ s is for $h_{\mathrm{max}} \approx 225$ km (Gustavsson et al., 2001) with $f_0 = 5.423$ MHz (Fig. 6).

With $f_0 = 6.200$ MHz, τ_{obs} for the 630.0 nm line is almost equal to $\tau_{\mathrm{O(^1D)}}$. For the 557.7 nm line, τ_{obs} is approximately four
165   times larger than $\tau_{\mathrm{O(^1S)}}$. These results suggest that for $f_0 = 6.200$ MHz, the excitation sources Q_α for both emissions reach their maximum faster than $\tau_{\mathrm{O(^1D)}} \approx 40$ s but slower than $\tau_{\mathrm{O(^1S)}} \approx 1.3$ s, and probably the source growth rates are different for the two emissions.

On the other hand, with $f_0 = 5.423$ MHz, τ_{obs} for b oth emissions is several times larger than τ_α. In addition, τ_{obs} for both emissions is larger than with $f_0 = 6.200$ MHz. This suggests that for $f_0 = 5.423$ MHz, the source Q_α increases during
170   pumping, and slower than for $f_0 = 6.200$ MHz. A relatively slow growth of emissions at 557.7 nm has also been observed in experiments at the HAARP facility with $f_0 = 7.8$ MHz and an ERP of approximately 160 MW (Pedersen et al., 2003). The 557.7 to 630.0 nm intensity ratio in that case was approximately 1:3.

5   Discussion

Excitation of the O(^{1}D) state, the source of the 630.0 nm line, has been attributed to mainly electron heating from a maxwellian
175   electron distribution (Mantas, 1994; Mantas and Carlson, 1996), however, taking into account collisional de-excitation by collisions with molecular oxygen and nitrogen in the atmosphere (Gustavsson et al., 2001). The association of the 630.0 nm emissions with electron heating is consistent with our results for the optical (Fig. 2) and electron temperature enhancements (Fig. 4). Both decreased when f_0 was changed from 6.200 to 5.423 MHz at about 16:51 UT.

HF pump-enhanced optical emissions have been connected to upper hybrid waves because the emission intensities are
180   sensitive to f_0 near sf_{e} (Kosch et al., 2002a; Gustavsson et al., 2006). The response of ionospheric F-region plasma to HF pumping is asymmetric around sf_{e} (Leyser et al., 1989; Stubbe et al., 1994; Honary et al., 1995; Gustavsson et al., 2006). This is related to asymmetries in the dispersion characteristics of upper hybrid and electron Bernstein modes for frequencies near sf_{e} and $s \geq 3$. Theories of the localization of upper hybrid oscillations in density depletions of filamentary density striations along the geomagnetic field predict an asymmetry in the trapping mechanism with deeper depletions for $f_0 \gtrsim sf_{\mathrm{e}}$ than for
185    $f_0 \lesssim sf_{\mathrm{e}}$ (Mjølhus, 1993). Therefore stronger pump-induced effects are expected for $f_0 \gtrsim sf_{\mathrm{e}}$ than for $f_0 \lesssim sf_{\mathrm{e}}$ which gives a corresponding asymmetry also in the anomalous absorption of HF waves by scattering on the striations (Honary et al., 1995; Gurevich et al., 1996) and electron acceleration by the localized upper hybrid oscillations (Istomin and Leyser, 2003). These phenomena are expected to be correlated with electron temperature enhancements which are the source of optical emissions at

630.0 nm and which therefore too are expected to be stronger for $f_0 \gtrsim s f_e$ than for $f_0 \lesssim s f_e$. With $f_0 \approx s f_e$, upper hybrid and

190   electron Bernstein phenomena are suppressed because of the linear dispersion characteristics.

In order to find out the relation between $f_0 = 5.423$ MHz and $4 f_e$ in our experiment, we use the IGRF model (International Geomagnetic Reference Field, 13th generation) for the altitude variation of the geomagnetic field in the pump–ionosphere interaction region. We find that $4 f_e \approx f_0 = 5.423$ MHz occurred at the height of $h \approx 235$ km for the date of our experiment. This altitude is above that for the maximum volume emission rates at both 630.0 and 557.7 nm. Figure 6 shows this height to be

195    $h_{\max} \approx 227$ km for 630.0 nm and $h_{\max} \approx 219$ km for 557.7 nm. Since f_e increases with decreasing altitude, we conclude that $f_0 < 4 f_e$ in the regions with maximum volume emission rates. The IGRF model gives for the 630.0 nm emissions, $f_e \approx 1.360$ MHz at $h_{\max} \approx 227$ km, so that $\Delta f \equiv f_0 - 4 f_e \approx -17$ kHz. For the emissions at 557.7 nm, $f_e \approx 1.364$ MHz at $h_{\max} \approx 219$ km, giving $\Delta f \approx -33$ kHz.

Stimulated electromagnetic emissions can also be used to estimate the vicinity of f_0 to $s f_e$ (Leyser, 2001), but in our

200   experiment the emissions were generally too weak for spectral structure to be identified. However, for the fourth HF pulse at $f_0 = 5.423$ MHz, a weak broad upshifted maximum (BUM) can be identified. In Fig. 4 it can be seen that the electron temperature is slightly more enhanced in the fourth (and last) HF pulse than in the preceding pulses at $f_0 = 5.423$ MHz, which indicates a stronger plasma excitation in the last pulse. For $s = 4$, the BUM has been observed in the range $4 f_e - 20$ kHz $\lesssim f_0 \lesssim 4 f_e + 120$ kHz (Frolov et al., 1998), thus mainly at $f_0 \gtrsim 4 f_e$. As f_e decreases with increasing altitude, the weak BUM

205   could have been excited at higher altitudes where $f_0 \gtrsim 4 f_e$ compared to where the optical emissions were enhanced. Also, we note that the height profiles in Figs. 5 and 6 are for the third HF pulse for which the quality of the optical data is higher than for the fourth pulse. The pump–plasma interaction altitudes may have changed slightly between the two pulses.

Gustavsson and Eliasson (2008) discussed pump-enhanced optical emissions at 427.8, 557.7, 630.0 and 844.6 nm for $f_0 = 5.423$ MHz and cycling the pump wave 4 min on/2 min off. By fitting observed optical emissions and modelled en-

210   hanced electron fluxes they obtained estimates of the volume emission rates for the different optical lines. They found that the maximum volume emission rate for all spectral lines occurred at approximately the same altitude (their figure 7), which agrees with our observations for $f_0 = 6.200$ MHz (Fig. 5). Also, the ratio of the column emission rates for the emissions at 557.7 and 630.0 nm varied in the range $I_{5577}/I_{6300} \approx 0.1$–0.4 during the experiment (from their figure 2), which agrees with our ratio for the same emission lines $I_{5577}/I_{6300} \approx 0.2$, but again at $f_0 = 6.200$ MHz. In our case with $f_0 = 5.423$ MHz, the maximum

215   of the emissions at 557.7 nm occurred about 7–10 km below that at 630.0 nm (Fig. 6). Further, the ratio $I_{5577}/I_{6300} \approx 0.5$ is slightly higher than that for the same emission lines presented by Gustavsson and Eliasson (2008) for $f_0 = 5.423$ MHz.

Gustavsson and Eliasson (2008) found the maximum volume emission rate for 630.0 and 557.7 nm at $h_{\max} \approx 220$ km and higher, depending on time in the experiment (their figure 7). According to the IGRF model for the date of their experiments, $4 f_e \approx 5.414$ MHz at 220 km and lower at increasing altitudes. Thus, in their case $f_0 \gtrsim 4 f_e$ in the height region with the main

220   pump-enhanced optical emissions. In view of the similarities between the results of Gustavsson and Eliasson (2008) and our case with $f_0 = 6.200$ MHz, together with that in our case $f_0 = 5.423$ MHz $\lesssim 4 f_e$ at the altitudes of maximum volume emission rates as discussed above, we conjecture that $f_0 = 5.423$ MHz $\lesssim 4 f_e$ in the regions where the optical emissions were enhanced in our experiment.

Further, the dispersion characteristics of upper hybrid waves (Leyser et al., 1989; Istomin and Leyser, 1995; Mishin et al.,
225   2005) are similar for the case of Gustavsson and Eliasson (2008) with $f_0 = 5.423$ MHz $\gtrsim 4f_e$ and our case for $f_0 = 6.200$
MHz $\approx 4.6 f_e$. In both cases, upper hybrid waves can have a wide range of wave numbers, which facilitates large electron
temperature enhancements and emissions at 630.0 nm. On the other hand, for $f_0 \lesssim 4f_e$, as in our case for $f_0 = 5.423$ MHz,
upper hybrid waves with positive group dispersion are limited to relatively small wave numbers only which is expected to
give less electron heating and lower emission levels at 630.0 nm. Therefore, our result of $I_{5577}/I_{6300} \approx 0.5$ appears consistent
230   with $I_{5577}/I_{6300} \approx 0.1$–0.4 as observed by Gustavsson and Eliasson (2008), both with $f_0 = 5.423$ MHz but the former with
$f_0 \lesssim 4f_e$ and the latter with $f_0 \gtrsim 4f_e$.

The fact that the column emission rate at 630.0 nm in our case decreased when f_0 was lowered from $f_0 = 6.200$ to $f_0 =$
5.423 MHz is consistent with the theoretically predicted asymmetry in pump-induced effects for f_0 around $4f_e$, with weaker
enhancements for $f_0 \lesssim 4f_e$ and the largest excitations for $f_0 \gtrsim 4f_e$. For $f_0 = 6.200$ MHz $\approx 4.6f_e$, the excitation level should
235   be somewhere in between these two cases, that is, stronger than for $f_0 = 5.423$ MHz $\lesssim 4f_e$, as observed. However, we note
that no such asymmetry in the 630.0 nm emission has been observed in previous experiments (Gustavsson et al., 2006; Shindin
et al., 2015), although the emission intensity is minimum for $f_0 \approx s f_e$.

Emissions at 557.7 nm have been interpreted in terms of electron acceleration giving a non-thermal tail in the electron
distribution, rather than electron heating (Gustavsson et al., 2002, 2005). Istomin and Leyser (2003) presented a model of
240   electron acceleration by upper hybrid oscillations localized in the density depletion of a striation pumped by a left-handed
circularly polarized electromagnetic wave, that gives a power-law tail in the electron velocity distribution. From their equation
(40) we obtain an estimate of the maximum possible upper hybrid wave number perpendicular to the geomagnetic field for
$\Delta f \approx -33$ kHz (557.7 nm) as $k_{\perp \mathrm{max}} \rho_e \approx 0.1$, where ρ_e is the thermal electron gyro radius. With an electron temperature
of 2500 K (Fig. 4), $\rho_e \approx 0.023$ m, which gives $k_{\perp \mathrm{max}} \approx 5$ m^{-1} or upper hybrid wavelengths longer than about 1 m. For
245   $\Delta f \approx -17$ kHz (630.0 nm), $k_{\perp \mathrm{max}}$ is even smaller which implies an even smaller range of possible upper hybrid wavelengths.
For wave numbers $k_\perp \gtrsim k_{\perp \mathrm{max}}$, upper hybrid waves have negative group dispersion for which the waves cannot be localized
in density depletions and therefore can only be relatively weakly excited.

As the 557.7 nm column emission rate in our case was approximately the same or even increased as f_0 was decreased, we
conclude that this emission is excited through electron acceleration by relatively long upper hybrid wavelengths, about 1 m or
250   longer that can be excited for $f_0 = 5.423$ MHz $\lesssim 4f_e$ as well as for $f_0 = 6.200$ MHz. This assumes that the pump-induced
electron energization occurred approximately at the altitudes where the optical volume emission rates are the largest. The slow
growth of the 557.7 nm line relative to the lifetime of the O(^{1}S) state (Table 1) is consistent with the fact that upper hybrid
waves need to be localized in the slowly growing density depletions of striations for efficient electron acceleration. The fact
that both the 630.0 and 557.7 nm emissions exhibited a much longer growth time than the lifetime of the corresponding excited
255   states is consistent with the relatively weak level of upper hybrid phenomena that is expected for $f_0 \lesssim 4f_e$ where only relatively
long wavelengths can be excited.

The emission intensity at 557.7 nm for $f_0 = 5.423$ MHz was relatively high despite the lower ERP and the expected limited
wavelength range of upper hybrid oscillations. This can be understood by the assumption that the anomalous absorption of the

pump wave (and associated electron temperature enhancements) decreased as f_0 was lowered from 6.200 MHz to 5.423 MHz,
260   thereby giving stronger pumping of the long-wavelength upper hybrid oscillations for electron acceleration. Conversely, the
larger enhancements of both the 630.0 nm intensity and the electron temperature for $f_0 = 6.200$ MHz are attributed to mainly
the wider range of upper hybrid wavelengths that are available compared to that for $f_0 = 5.423$ MHz $\lesssim 4f_e$, in addition to the
slightly higher ERP.

Kvammen et al. (2019) concluded for the same experiment that $f_0 = 5.423$ MHz $\gtrsim 4f_e$ by comparing their observed increase
265   in the enhancement at 844.6 nm (10.99 eV threshold) for $f_0 = 5.423$ MHz to Gustavsson et al. (2006) who observed larger
enhancements at 427.8 nm (18.75 eV threshold) for $f_0 \gtrsim 4f_e$ than for $f_0 \lesssim 4f_e$. We note that the ERP in the experiments by
Gustavsson et al. (2006) was four to five times higher than in the present experiment, implying that a comparison between the
experiments may not be obvious. In view of that $f_0 = 5.423$ MHz $\lesssim 4f_e$ at the altitudes of maximum volume emission rates
we suggest the possibility that $f_0 \lesssim 4f_e$ in the excitation regions of the optical emissions. With $f_0 \lesssim 4f_e$. at lower altitudes
270   and $f_0 \gtrsim 4f_e$ at higher altitudes, there would be a region with $f_0 \approx 4f_e$ in between with minimum pump–plasma interaction
involving upper hybrid and electron Bernstein modes, therefore minimum electron heating and enhancements at 630.0 nm.
With f_0 sufficiently near $4f_e$, regardless of wether $f_0 \lesssim 4f_e$ or $f_0 \gtrsim 4f_e$, upper hybrid and electron Bernstein oscillations
would have only relatively long wavelengths, which are suggested to be involved in the electron acceleration that enhances
emissions at 557.7 nm, (and 844.6 nm as studied by Kvammen et al. (2019)).

275   Najmi et al. (2017) presented results from Vlasov and test-particle simulations that indicate the physics of electron energiza-
tion by wave modes perpendicular to the ambient magnetic field and trapped in the density depletion of a striation in the upper
hybrid resonance region. When f_0 is between $3f_e$ and $4f_e$, bulk electron heating occurs by electron Bernstein waves which
leads to an essentially thermal electron velocity distribution. For $f_0 \gtrsim 4f_e$, resonant interaction with the upper hybrid mode
was found to dominate which leads to electron acceleration and the formation of a suprathermal tail of energetic electrons.
280   However, with $f_0 = 4.01f_e$ in their simulations, the frequency shift of f_0 above $4f_e$ is less than the lower hybrid frequency
they used. This implies that decay products of parametric interaction between upper hybrid oscillations at f_0 and lower hybrid
oscillations have frequencies below $4f_e$, so that the interaction involves upper hybrid waves both slightly above and below $4f_e$.
Their results can therefore not be used for a comparison of electron energization efficiency of $f_0 \lesssim 4f_e$ and $f_0 \gtrsim 4f_e$ as would
be relevant for the present study. But the importance of electron heating for f_0 not near sf_e is consistent with our result of
285   enhanced 630.0 nm emissions and electron temperatures for $f_0 = 6.200$ MHz.

Shindin et al. (2015) detected enhancements at 557.7 nm only for f_0 about 15–20 kHz above $4f_e$ in experiments at the
Sura facility, with the HF beam tilted 12° south from vertical in the magnetic meridional plane and the photometers directed in
magnetic zenith (19° south). For a vertical HF beam, emissions were observed with f_0 about 5–15 kHz below $4f_e$ and also at
about 220–280 kHz above $4f_e$. Our suggestion that the emission was enhanced for $f_0 \lesssim 4f_e$ with the Heating beam in magnetic
290   zenith thus agrees with Shindin et al. (2015) for a vertical Sura beam, but disagrees with their observations for the Sura beam
tilted towards magnetic zenith. However, we do not find it clear whether Shindin et al. (2015) actually obtained conditions with
$f_0 \lesssim 4f_e$ and the HF beam tilted towards magnetic zenith, so that a comparison with the observed 557.7 nm enhancements
for $f_0 \gtrsim 4f_e$ could actually be made. Further, although Shindin et al. (2015) by superposed epoch analysis convincingly bring

forth the pump-enhanced 557.7 nm emission, their data remains noisy with variations in the natural background airglow. The
experimental conditions in our case were better and the optical emissions were enhanced well above background. Another
point is that even with f_0 about 15–20 kHz above $4f_\mathrm{e}$ in some altitude region, enhancement of optical emissions could also
occur at some ten kilometers or more lower altitudes at which $f_0 \lesssim 4f_\mathrm{e}$.

Gustavsson et al. (2002) observed $I_{5577}/I_{6300} \approx 0.3$–0.4 for $f_0 = 4.040$ MHz which is near $3f_\mathrm{e}$, in experiments with
EISCAT-Heating and an ERP of approximately 73 MW. From estimates of the reflection altitude, the authors found that
$f_0 \lesssim 3f_\mathrm{e}$ in the early part of the experiment which changed to $f_0 \gtrsim 3f_\mathrm{e}$ in the later part because of the slowly increasing pump
reflection height during the evening. We note that the largest ratio $I_{5577}/I_{6300} \approx 0.4$ was observed in the early part of the
experiment (their figure 2), when $f_0 \lesssim 3f_\mathrm{e}$, which is consistent with our results with $f_0 = 5.423$ MHz $\lesssim 4f_\mathrm{e}$.

Kosch et al. (2005) presented experimental results from the HAARP facility and found $I_{5577}/I_{6300} \approx 0.2$–0.4, but for $f_0 \gtrsim$
$3f_\mathrm{e}$ (their figure 1). We note that the largest ratio $I_{5577}/I_{6300} \approx 0.4$ was observed in the first displayed pump pulse when f_0
was the closest to $3f_\mathrm{e}$. The ERP was 47.8 MW. However, no results were obtained for $f_0 \lesssim 3f_\mathrm{e}$ to compare with. Thus, Kosch
et al. (2005) observed the largest ratio $I_{5577}/I_{6300} \approx 0.4$ for $f_0 \gtrsim 3f_\mathrm{e}$, while Gustavsson et al. (2002) observed their largest
ratio $I_{5577}/I_{6300} \approx 0.4$ for $f_0 \lesssim 3f_\mathrm{e}$. In addition, the ERP was larger in the experiment by Gustavsson et al. (2002) than for
Kosch et al. (2005). One difference between these two experiments that may have influenced the excitation efficiency for the
optical emissions is that Gustavsson et al. (2002) used a vertically transmitted pump beam while Kosch et al. (2005) transmitted
the beam in magnetic zenith where maximum optical effects are expected (Kosch et al., 2000; Pedersen and Carlson, 2001;
Pedersen et al., 2008). This could have contributed to the high ratio I_{5577}/I_{6300} for $f_0 \gtrsim 3f_\mathrm{e}$ observed by Kosch et al. (2005)
despite the lower ERP.

6 Conclusions

The EISCAT Heating facility was used to excite ionospheric F-region plasma by HF pumping 150 s on/85 s off and the beam
pointing in geomagnetic zenith, with $f_0 = 6.200$ MHz followed by $f_0 = 5.423$ MHz. Optical emissions imaged at 557.7 and
630.0 nm from three ALIS stations were analyzed and plasma parameter values were obtained with the EISCAT UHF inco-
herent scatter radar. From tomography-like reconstruction of the altitude distribution of the optical volume emission rates, we
conclude that $f_0 = 6.200$ MHz $\approx 4.6f_\mathrm{e}$ and $f_0 = 5.423$ MHz $\lesssim 4f_\mathrm{e}$ in the height regions with the largest optical enhance-
ments. The ratio of the column emission rates was $I_{5577}/I_{6300} \approx 0.2$ with $f_0 = 6.200$ MHz. As f_0 was decreased to 5.423
MHz, the pump-induced enhancements of both the 630.0 nm emissions and electron temperature decreased. This is consistent
with that the O(^{1}D) state is excited mainly by electron heating. On the other hand, the emission intensity at 557.7 nm was
approximately the same or even increased slightly as f_0 was decreased to 5.423 MHz, so that $I_{5577}/I_{6300} \approx 0.5$. The 557.7
nm enhancement is suggested to depend primarily on upper hybrid waves with wavelengths of 1 m or longer that can be
excited for $f_0 = 5.423$ MHz $\lesssim 4f_\mathrm{e}$. The fact that the growth times of both emissions in this case were several times longer
than the lifetimes of the respective excited states, indicates that both emissions depend on the formation of small-scale density
striations, which is expected to be slower for $f_0 \lesssim 4f_\mathrm{e}$ than for f_0 not near sf_e ($s \geq 3$).

Data availability. Access to the raw data may be provided upon reasonable request to the authors.

Author contributions. TBL organized the experiment, interpreted the results and wrote the paper. TS analysed the data, did the theoretical modeling and provided the plots for the figures. All took part in the experiment and contributed to the paper.

330 *Competing interests.* The authors declare that they have no conflict of interest.

Acknowledgements. EISCAT is an international association supported by research organizations in China (CRIRP), Finland (SA), Japan (NIPR and ISEE), Norway (NFR), Sweden (VR), and the United Kingdom (UKRI).

References

Brändström, B. U. E., Leyser, T. B., Steen, Å., Rietveld, M. T., Gustavsson, B., Aso, T., and Ejiri, M.: Unambiguous evidence of HF pump-enhanced airglow at auroral latitudes, Geophys. Res. Lett., 26, 3561–3564, https://doi.org/https://doi.org/10.1029/1999GL010693, 1999.

Frolov, V. L., Ekukhimov, L. M., Kagan, L. M., Komrakov, G. P., Sergeev, E. N., and Stubbe, P.: Two-component nature of the broad up-shifted maximum in stimulated electromagnetic emission spectra, Phys. Rev. Lett., 81, 1630–1633, https://doi.org/https://doi.org/10.1103/PhysRevLett.81.1630, 1998.

Grach, S. M., Kosch, M. J., Yashnov, V. A., Sergeev, E. N., Atroshenko, M. A., and Kotov, P. V.: On the location and structure of the artificial 630-nm airglow patch over Sura facility, Annales Geophysicae, 25, 689–700, https://doi.org/10.5194/angeo-25-689-2007, 2007.

Gurevich, A. V., Lukyanov, A. V., and Zybin, K. P.: Anomalous absorption of powerful radio waves on the striations developed during ionospheric modification, Phys. Lett. A, 211, 363–372, https://doi.org/https://doi.org/10.1016/0375-9601(95)00970-1, 1996.

Gustavsson, B. and Eliasson, B.: HF radio wave acceleration of ionospheric electrons: Analysis of HF-induced optical enhancements, Journal of Geophysical Research: Space Physics, 113, https://doi.org/https://doi.org/10.1029/2007JA012913, 2008.

Gustavsson, B., Sergienko, T., Rietveld, M. T., Honary, F., Steen, Å., Brändström, B. U. E., Leyser, T. B., Arulia, A., Aso, T., and Ejiri, M.: First tomographic estimate of volume distribution of enhanced airglow emission caused by HF pumping, J. Geophys. Res., 106, 29 105–29 123, https://doi.org/10.1029/2000JA900167, 2001.

Gustavsson, B., Brändström, B. U. E., Steen, Å., Sergienko, T., Leyser, T. B., Rietveld, M. T., Aso, T., and Ejiri, M.: Nearly simultaneous images of HF pump-enhanced airglow at 6300 Å and 5577 Å, Geophys. Res. Lett., 29, https://doi.org/10.1029/2002GL015350, 2002.

Gustavsson, B., Sergienko, T., Kosch, M. J., Rietveld, M. T., Brändström, B. U. E., Leyser, T. ., Isham, B., Gallop, P., Aso, T., Ejiri, M., Grydeland, T., Steen, A., LaHoz, C., Kaila, K., Jussila, J., and Holma, H.: The electron energy distribution during HF pumping, a picture painted with all colors, Ann. Geophys., 23, 1747–1754, https://doi.org/https://doi.org/10.5194/angeo-23-1747-2005, 2005.

Gustavsson, B., Leyser, T. B., Kosch, M., Rietveld, M. T., Steen, A., Brändström, B. U. E., and Aso, T.: Electron Gyroharmonic Effects in Ionization and Electron Acceleration during High-Frequency Pumping in the Ionosphere, Phys. Rev. Lett., 97, 195 002, https://doi.org/10.1103/PhysRevLett.97.195002, 2006.

Haslett, J. C. and Megill, L. R.: A model of the enhanced airglow excited by RF radiation, Radio Sci., 9, 1005–1019, https://doi.org/https://doi.org/10.1029/RS009i011p01005, 1974.

Holma, H., Kaila, K., Kosch, M., and Rietveld, M.: Recognizing the blue emission in artificial aurora, Adv. Space Res., 38, 2653–2658, https://doi.org/10.1016/j.asr.2005.07.036, 2006.

Honary, F., Stocker, A. J., Robinson, T. R., Jones, T. B., and Stubbe, P.: Ionospheric plasma response to HF radio waves operating at frequencies close to the third harmonic of the electron gyrofrequency, J. Geophys. Res., 100, 21 489–21 501, https://doi.org/https://doi.org/10.1029/95JA02098, 1995.

Istomin, Y. N. and Leyser, T. B.: Parametric decay of an electromagnetic wave near electron cyclotron harmonics, Phys. Plasmas, 2, 2084–2097, https://doi.org/https://doi.org/10.1063/1.871295, 1995.

Istomin, Y. N. and Leyser, T. B.: Electron acceleration by cylindrical upper hybrid oscillations trapped in density irregularities in the ionosphere, Physics of Plasmas, 10, 2962–2970, https://doi.org/https://doi.org/10.1063/1.1578637, 2003.

Kosch, M. J., Rietveld, M. T., Hagfors, T., and Leyser, T. B.: High-latitude HF-induced airglow displaced equatorwards of the pump beam, Geophys. Res. Lett., 27, 2817–2820, https://doi.org/10.1029/2000GL003754, 2000.

Kosch, M. J., Rietveld, M. T., Kavanagh, A. J., Davies, C., Yeoman, T. K., Honary, F., and Hagfors, T.: High-latitude
pump-induced optical emissions for frequencies close to the third electron gyro-harmonic, Geophys. Res. Lett., 29, 2112,
https://doi.org/10.1029/2002GL015744, 2002a.

Kosch, M. J., Rietveld, M. T., Yeoman, T. K., Cierpa, K., and Hagfors, T.: The high-latitude artificial aurora of 21 February 1999: An analysis,
Adv. Polar Upper Atmos. Res., 16, 1–12, 2002b.

Kosch, M. J., Rietveld, M. T., Senior, A., McCrea, I. W., Kavanagh, A. J., Isham, B., and Honary, F.: Novel artificial optical annular structures
in the high latitude ionosphere over EISCAT, Geophys. Res. Lett., 31, L12 805, https://doi.org/:10.1029/2004GL019713, 2004.

Kosch, M. J., Pedersen, T., Hughes, J., Marshall, R., Gerken, E., Senior, A., Sentman, D., McCarrick, M., and Djuth, F. T.: Artificial op-
tical emissions at HAARP for pump frequencies near the third and second electron gyro-harmonic, Ann. Geophys., 23, 1585–1592,
https://doi.org/10.5194/angeo-23-1585-2005, 2005.

Kosch, M. J., Pedersen, T., Mishin, E., Starks, M., Gerken-Kendall, E., Sentman, D., Oyama, S., and Watkins, B.: Temporal evo-
lution of pump beam self-focusing at the High-Frequency Active Auroral Research Program, J. Geophys. Res., 112, A08 304,
https://doi.org/10.1029/2007JA012264, 2007.

Kvammen, A., Gustavsson, B., Sergienko, T., Brändström, U., Rietveld, M., Rexer, T., and Vierinen, J.: The 3-D Distribution of Ar-
tificial Aurora Induced by HF Radio Waves in the Ionosphere, Journal of Geophysical Research: Space Physics, 124, 2992–3006,
https://doi.org/https://doi.org/10.1029/2018JA025988, 2019.

Leyser, T. B.: Stimulated electromagnetic emissions by high-frequency electromagnetic pumping of the ionospheric plasma, Space Sci. Rev.,
98, 223–328, https://doi.org/10.1023/A:1013875603938, 2001.

Leyser, T. B., Thidé, B., Derblom, H., Hedberg, Å., Lundborg, B., Stubbe, P., and Kopka, H.: Stimulated electromagnetic emission near elec-
tron cyclotron harmonics in the ionosphere, Phys. Rev. Lett., 63, 1145–1147, https://doi.org/https://doi.org/10.1103/PhysRevLett.63.1145,
1989.

Mantas, G. P.: Large 6300-Åairglow intensity enhancements observed in Ionosphere Heating Experiments are excited by thermal electrons,
Journal of Geophysical Research: Space Physics, 99, 8993–9002, https://doi.org/https://doi.org/10.1029/94JA00347, 1994.

Mantas, G. P. and Carlson, H. C.: Reinterpretation of the 6300-Å airglow enhancements observed in ionospheric heating experiments based
on analysis of Platteville, Colorado, data, J. Geophys. Res., 101, 195–209, https://doi.org/https://doi.org/10.1029/95JA02760, 1996.

Mishin, E. V., Kosch, M. J., , Pedersen, T., and Burke, W. J.: HF-induced airglow at magnetic zenith: Thermal and parametric instabilities
near electron gyroharmonics, Geophys. Res. Lett., 32, L23 106, https://doi.org/10.1029/2005GL023864, 2005.

Mjølhus, E.: On the small scale striation effect in ionospheric radio modification experiments near harmonics of the electron gyro frequency,
J. Atmos. Terr. Phys., 55, 907–918, https://doi.org/https://doi.org/10.1016/0021-9169(93)90030-3, 1993.

Najmi, A., Eliasson, B., Shao, X., Milikh, G., Sharma, A. S., and Papadopoulos, K.: Vlasov simulations of electron acceleration by radio
frequency heating near the upper hybrid layer, Physics of Plasmas, 24, 102 904, https://doi.org/10.1063/1.4999768, 2017.

Pedersen, T., Esposito, R., Starks, M., and McCarrick, M.: Quantitative determination of HF radio-induced optical emission production
efficiency at high latitudes, J. Geophys. Res., 113, A11 316, https://doi.org/10.1029/2008JA013502, 2008.

Pedersen, T. R. and Carlson, H. C.: First observations of HF heater-produced airglow at the High Frequency Active Auroral Research Program
facility: Thermal excitation and spatial structuring, Radio Sci., 36, 1013–1026, https://doi.org/10.1029/2000RS002399, 2001.

Pedersen, T. R., McCarrick, M., Gerken, E., Selcher, C., Sentman, D., Carlson, H. C., and Gurevich, A.: Magnetic zenith enhancement of
HF radio-induced airglow production at HAARP, Geophys. Res. Lett., 30, 1169, https://doi.org/10.1029/2002GL016096, 2003.

Rietveld, M. T., Senior, A., Markkanen, J., and Westman, A.: New capabilities of the upgraded EISCAT high-power HF facility, Radio Sci., 51, 1533–1546, https://doi.org/10.1002/2016RS006093, 2016RS006093, 2016.

Sergienko, T., Gustavsson, B., Brändström, U., and Axelsson, K.: Modelling of optical emissions enhanced by the HF pumping of the ionospheric F-region, Ann. Geophys., 30, 885–895, https://doi.org/10.5194/angeo-30-885-2012, 2012.

410   Shindin, A., Grach, S. M., Klimenk, V. V., Nasyrov, I. A., Sergeev, E. N., Beletski, A. B., Taschilin, M. A., and I.Gumerov, R.: The 630 nm and 557.7 nm Airglow During HF Ionosphere Pumping by the SURA Facility Radiation for Pump Frequencies Near the Fourth Electron Gyroharmonic, Radiophys. Quantum Electron., 57, 759–772, https://doi.org/10.1007/s11141-015-9562-9, 2015.

Stubbe, P., Stocker, A. J., Honary, F., Robinson, T. R., and Jones, T. B.: Stimulated electromagnetic emission and anomalous HF wave absorption near electron gyroharmonics, J. Geophys. Res., 99, 6233–6246, https://doi.org/https://doi.org/10.1029/94JA00023, 1994.